Variability of Vascular Reactivity in the Retina and Choriocapillaris to Oxygen and Carbon Dioxide Using Optical Coherence Tomography Angiography

Bright S. Ashimatey,[1] Xiao Zhou,[2] Zhongdi Chu,[2] Muhammed Alluwimi,[1] Ruikang K. Wang,[2,3] and Amir H. Kashani[1]

[1]Wilmer Eye Institute, Johns Hopkins School of Medicine, Baltimore, Maryland, United States
[2]Department of Bioengineering, University of Washington, Seattle, Washington, United States
[3]Department of Ophthalmology, University of Washington Seattle, Washington, United States

Correspondence: Amir H. Kashani, Wilmer Eye Institute, Johns Hopkins School of Medicine, 600 North Wolfe Street, Baltimore, MD 21287, USA; akashan1@jhmi.edu.

Received: September 25, 2022
Accepted: January 11, 2023
Published: February 6, 2023

Citation: Ashimatey BS, Zhou X, Chu Z, Alluwimi M, Wang RK, Kashani AH. Variability of vascular reactivity in the retina and choriocapillaris to oxygen and carbon dioxide using optical coherence tomography angiography. *Invest Ophthalmol Vis Sci.* 2023;64(2):9. https://doi.org/10.1167/iovs.64.2.9

Purpose. To investigate the regional and layer-specific vascular reactivity of the healthy human retina and choriocapillaris to changes in systemic carbon dioxide or oxygen.

Methods. High-resolution 3 × 3-mm^2 optical coherence tomography angiography (OCTA) images were acquired from the central macula, temporal macula, and peripapillary retina while participants were exposed to three gas breathing conditions—room air, 5%CO_2, and 100% O_2. OCTA from all three regions were extracted and the apparent skeletonized vessel density (VSD) was assessed. The mean flow deficit sizes (MFDSs) of the choriocapillaris were also assessed. Repeated-measures analysis of variance was used to compare the ratio of intrasubject VSD change induced by the gas conditions from baseline in the superficial retinal layer (SRL) and deep retinal layer (DRL) for each retinal region independently, as well as the MFDS of the choriocapillaris. We also compared the vessel reactivity between the retinal capillaries and the choriocapillaris.

Results. The cumulative intrasubject response to the gas conditions differed significantly among regions of the SRL ($F(2, 7) = 28.22$, $P < 0.001$), with the temporal macula showing the largest response (15%) compared to the macula (8%) and radial peripapillary capillaries (7%). A similar trend was found in the DRL. The choriocapillaris reactivity was similar between the macula (5.8%) and temporal macula (5.6%). There was also a significant heterogeneity in the layer-specific gas responses, with the DRL showing the largest response (28.2%) and the choriocapillaris showing the smallest response (2.8%).

Conclusions. Capillary reactivity to changes in inhaled O_2 and CO_2 is spatially heterogeneous across the retina but not choriocapillaris.

Keywords: retina, capillary, choriocapillaris, reactivity, oxygen, carbon dioxide, optical coherence tomography angiography

The retina has one of the most specialized circulatory systems of the human body. Its high metabolic demand and need for optical transparency is met by a bipartite vascular system in which the inner retinal layers are supplied by the central retinal branch of the ophthalmic artery and the outer retina by the posterior ciliary arteries.[1] These two vascular systems of the posterior segment are distinctly different in their microstructure as well as function.[2,3] The retinal vasculature also has significant morphologic and functional heterogeneity. Morphologic heterogeneity is illustrated by distinct appearances of the superficial, deep, peripapillary retinal capillaries and choriocapillaris[4–6] as well as the appearance of endothelial cells in different vascular segments.[7] Functional heterogeneity is demonstrated by electrophysiologic studies of pericyte function from different vascular segments.[8] This heterogeneity may contribute to the preferential involvement of retinopathy in one retinal region over another in diseases such as diabetic retinopathy, sickle cell retinopathy, and ocular ischemic syndrome.[9–11] For example, diabetic retinopathy is localized primarily to the posterior segment,[12,13] whereas sickle cell retinopathy is primarily peripheral.[14]

In addition, there is evidence of differential susceptibility of the deep capillary layer in the early phases of diabetic retinopathy and hypertension,[15–18] and the superficial retinal layer shows greater abnormality in the late phases of diabetes.[19] Both retinal and choroidal circulations show abnormality in central serous retinopathy.[20] Similarly, in glaucoma, abnormal perfusion in the peripapillary capillaries may play an important role in the onset and progression of the disease.[21,22] A better understanding of the spatial characteristics of the retinal microvasculature, as well as their response to physiologically relevant stimuli, may be useful for understanding the different disease susceptibilities and mechanisms.

Assessing the vascular alterations of the retina requires simultaneous assessment of both retinal capillaries and choriocapillaris. Our study applies optical coherence

tomography angiography (OCTA) imaging to characterize physiologically relevant perfusion changes in the retina over spatially and morphologically distinct regions of vasculature in the posterior pole, specifically in response to inhalation of elevated levels of oxygen or carbon dioxide. We utilize gas inhalation methods that have been demonstrated to reliably elicit significant changes in human retinal vascular reactivity[18,20,23,24] and human cerebrovascular reactivity,[25,26] and they are being used in multicenter human studies assessing biomarkers of cerebrovascular reactivity.[20,27] We hypothesize that the choriocapillaris and the superficial, deep, and peripapillary retinal capillaries of different retinal regions vary in the magnitude and nature of their vasomotor response to inhalation of oxygen and carbon dioxide. We use OCTA to characterize simultaneous changes in all these networks to better understand the local regulation of blood supply to the retina.

Materials and Method

Study Participants and Ethical Consideration

This was a single-arm, prospective, and observational study. The study adhered to the tenets of the Declaration of Helsinki and was approved by the institutional review board of the University of Southern California and Johns Hopkins University. Participation inclusion criteria were healthy individuals with no history of cardiovascular disease, including diabetes or hypertension, and aged greater than 18 years. Participants were excluded if they had comorbid eye diseases, including age-related macular degeneration or glaucoma. Participants with significant medical history, including shortness of breath, lung disease, congestive heart failure, or recent hospitalizations, were excluded. Overall, eight healthy controls were recruited and participated in the study.

OCTA Imaging Protocol

Participants were imaged using a Swept Source-OCTA (SS-OCTA) platform (PLEX Elite 9000, version 2.0; Carl Zeiss Meditec, Dublin, CA, USA). The device has a center wavelength between 1040 and 1060 nm with sweeping range between 980 and 1120 nm. The imaging speed is 100 kHz with a B-scan repetition of 4. Per the manufacturer's manual, the A-scan depth of field is approximately 3.00 mm (in tissue) and has an axial optical resolution of 6.3 µm. The lateral (or transverse) optical resolution is estimated as ~20 µm at the retina. During a 3 × 3-mm^2 image acquisition, the device acquires 300 B-scans and yields a pixel resolution of ~10 µm in retinal tissue. Images for this study were acquired with the enhanced depth imaging feature activated, which allows for improved focusing of the image beneath the plane of the retinal pigment epithelium.

The OCTA images were acquired while the participants were breathing through a customized gas delivery apparatus described elsewhere.[23,24] Each imaging session lasted approximately 30 minutes. In brief, the gas delivery apparatus was composed of a Douglas bag containing specialized gas mixtures connected through a series of tubes to the participants. The tube connections had two valves—one three-way valve that allowed control of the source of air inflow to the tube system and one two-way nonrebreathing valve that compartmentalized the air in the tubing system from expired air. The apparatus allowed simultaneous gas-mixture delivery to the participant while OCTA images were being acquired.

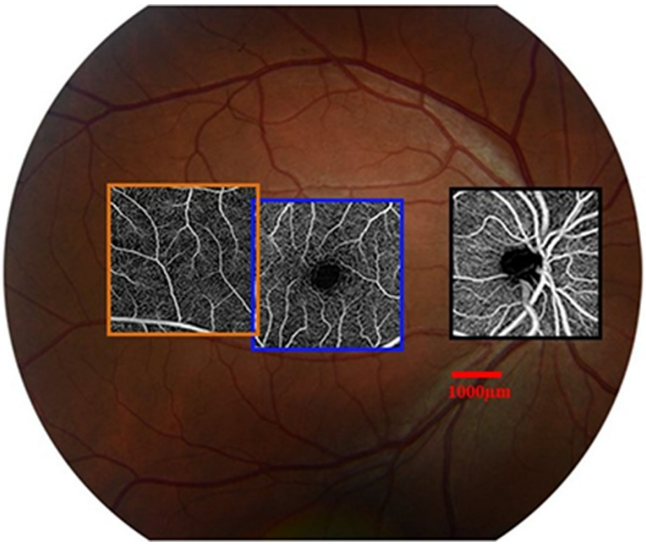

Figure 1. Fundus photograph with illustrative OCTA images from the retinal regions assessed in the study. The figure shows 3 × 3-mm^2 OCTA images of the retinal regions investigated and overlaid on a 50° color fundus image. The macula image was acquired with the participant gazing at the fixation target in the primary position. The temporal macula image was acquired in a similar manner with the image acquisition box displaced temporally to begin at the temporal border of the area covered by the macula image. The disc image was acquired by displacing the fixation target nasally and centering the image acquisition box over the optic disc. Each image was acquired in triplicate.

Each participant was asked to answer a study questionnaire to assess eligibility for the study as well as gather demographic and medical history data. Blood pressure of each participant was assessed in a sitting position. The participant's partial pressure of oxygen was assessed with a finger pulse oximetry probe, and participants with a baseline pulse oximeter reading lower than 98% were excluded. Proparacaine (0.5%), tropicamide (1%), and phenylephrine hydrochloride (2.5%) were instilled on the study eye to achieve pupillary dilation.

OCTA images were acquired under three gas nonrebreathing conditions for each participant. Nonrebreathing was achieved by use of a mouthpiece with a one-way valve and nose clip to prevent the participant from rebreathing exhaled air and is described in detail in Kushner-Lenhoff et al.[24] First, baseline OCTA images were acquired during room air (RA) breathing through the apparatus. OCTA images were acquired in triplicate at the macula, temporal macula, and disc region (Fig. 1). Participants were given a 2-minute break, and the three-way valve was switched to allow 5% CO_2 (mixed with 21% O_2 and 74% nitrogen) to be delivered through a nonrebreathing mouthpiece from a Douglas bag prefilled with the air mixture. After 60 seconds of the CO_2 nonrebreathing, another set of three OCTA images were acquired at the same retinal locations using the track-to-prior feature. The participant was then allowed a 10-minute rest to ensure clearance of the systemic CO_2 followed by OCTA imaging under 100% O_2 nonrebreathing in a manner similar to the CO_2 nonrebreathing.[4] All imaging sessions were performed in mesopic light conditions in the same room without any attempts to dark adapted or provide light stim-

Investigative Ophthalmology & Visual Science

ulation. Participants were allowed 20 minutes to adjust to the room lighting levels before imaging was performed.

The order of gas presentation (RA to CO_2 to O_2) was the same between participants. This design was to enhance efficiency and to the reduce the possibility of persistent gas effect of the prior condition on the succeeding condition. For instance, by acquiring baseline images at room air first, the need for a refractory period before room air imaging was eliminated. The possibility of a persistent gas effect from a prior gas condition on room air findings was also eliminated. Similarly, CO_2 breathing was assessed before O_2 to reduce the potential persistent O_2 effect beyond the 10-minute refractory period used in this study.[28] The order of retinal region imaging for any given participant was kept constant across gas conditions. However, this order was varied between participants to limit the potential influence of gas breathing duration on the results.

Participants were asked to stop the study if the study interventions caused more than minimal discomfort. Furthermore, the study procedures were halted if the pulse oximeter (which was constantly monitored during the study) read below 94% even if the participant was asymptomatic.

OCTA Image Analysis

One high-quality OCTA image per retinal region and gas condition was selected for analysis. High-quality images were defined as those with the fewest artifacts (including motion and segmentation artifacts) and highest signal strength. The superficial and deep retinal layers of the macula and temporal macula were extracted using the commercially available manufacturer software (PlexElite; Carl Zeiss Meditec). The superficial retinal layer included the nerve fiber layer, ganglion cell layer, and the inner nuclear layer. The deep retinal layer included the outer plexiform layer and less than 33% of the outer nuclear layer. Projection artifacts were excluded using the manufacturer software (PlexElite; Carl Zeiss Meditec).

The radial peripapillary capillaries were extracted using the maximum pixel projection customized slab setting with one boundary of the customized slab set to the inner limiting membrane (ILM) and the other displaced 75 µm below the ILM. The superficial 75 µm was used because the radial peripapillary capillaries were most visible and continuous at this depth in our case.[29]

The extracted vessel slabs were analyzed using a previously validated software that computed the apparent vessel skeleton density (VSD).[30,31] In brief, VSD is a linear measure of vessel length computed as the count of pixels representing vessels (after the OCTA image binarization and skeletonization) divided by the total number of pixels in the image. The software was modified for assessing SS-OCTA images and to coregister images from the different gas conditions. Nonoverlapping regions were excluded from the analysis. In addition, all noncapillary vessels (e.g., large caliber retinal arteries, veins, arterioles and venules) as well as their corresponding negative spaces were excluded from the analysis.[18] Anatomic regions known to be characterized by nonperfused OCTA signals (such as foveal avascular zone and disc region) were also excluded (Fig. 2).

The choriocapillaris images were also extracted from the macula and temporal macula scans. The Multilayer Segmentation algorithm version 0.7 (PlexElite; Carl Zeiss Meditec) was used to perform choriocapillaris segmentation, which was defined as a 16-µm-thick slab with its anterior boundary located 4 µm beneath Bruch's membrane.[32] En face choriocapillaris images were generated using maximum-intensity projection and projection artifact removal.[33] Flow deficit density (FDD) and mean flow deficit sizes (MFDSs) were computed for the choriocapillaris images using custom software. The flow deficits (FDs) were segmented from compensated choriocapillaris OCTA en face images as previously described.[34] Briefly, pixels were automatically clustered into different groups using the fuzzy C-means approach, and the cluster of pixels with the lowest intensity values was segmented as FDs. With segmented FDs, the choriocapillaris FDD and MFDS (μm^2) were calculated for the entire scan. The FDD was defined as the percentage of pixels representing FDs relative to the whole scan, and the MFDS was defined as the average size of all individual FDs in the whole scan.

Data Analysis

The data were analyzed to (1) characterize the distribution vessel density across the retinal regions studied, (2) assess the regional characteristics of the retinal vascular response to hyperoxia and hypercapnia, and (3) investigate the layer-specific response (including the choriocapillaris) to hyperoxia and hypercapnia. Specifically, changes in apparent VSD between gas conditions serve as a proxy for changes in perfusion of the underlying capillaries.

The regional measures of the VSD at baseline were compared between the superficial retinal layers of the macula and temporal macula, as well as the radial peripapillary capillaries using *F*-statistics from repeated-measures analysis of variance (ANOVA). The analysis was repeated for the VSD findings of the macula and temporal macula for the deep retina layer. The FDD and MFDS of the choriocapillaris were also compared between the macula and temporal macula regions.

The vascular response to the gas conditions was analyzed for a significant gas effect on the VSD also using a repeated-measures ANOVA. When there was an omnibus significant gas effect, the percent change from baseline was compared to investigate regional differences in the response to the gas conditions. The response to O_2 and CO_2 was assessed independently, as well as the cumulative gas effect that consisted of the overall VSD change induced by the O_2 and CO_2 gas conditions. The analyses were stratified based on the retinal layers. The analysis of the superficial layers included measures from the superficial macula, temporal macula, and the radial peripapillary capillaries. The analysis of the deep retinal layer and choriocapillaris included the macula and temporal macula.

The data analysis also included a comparison of the layer-specific responses to the gas conditions. Specifically, the analyses compared superficial and deep retinal layer findings and the choriocapillaris response to the gas conditions. In this analysis, the square root of the MFDS assessment of the choriocapillaris was used to enhance the similarity between the units of the retinal and choriocapillaris vascular response. The analysis also compensated for the effect of directionality of the choriocapillaris response, such as the response to O_2 in which the MFDS increased while the VSD of retinal capillaries decreased. The measures for the different layers were computed by averaging the findings from the macula and temporal macula regions for each layer.

Investigative Ophthalmology & Visual Science

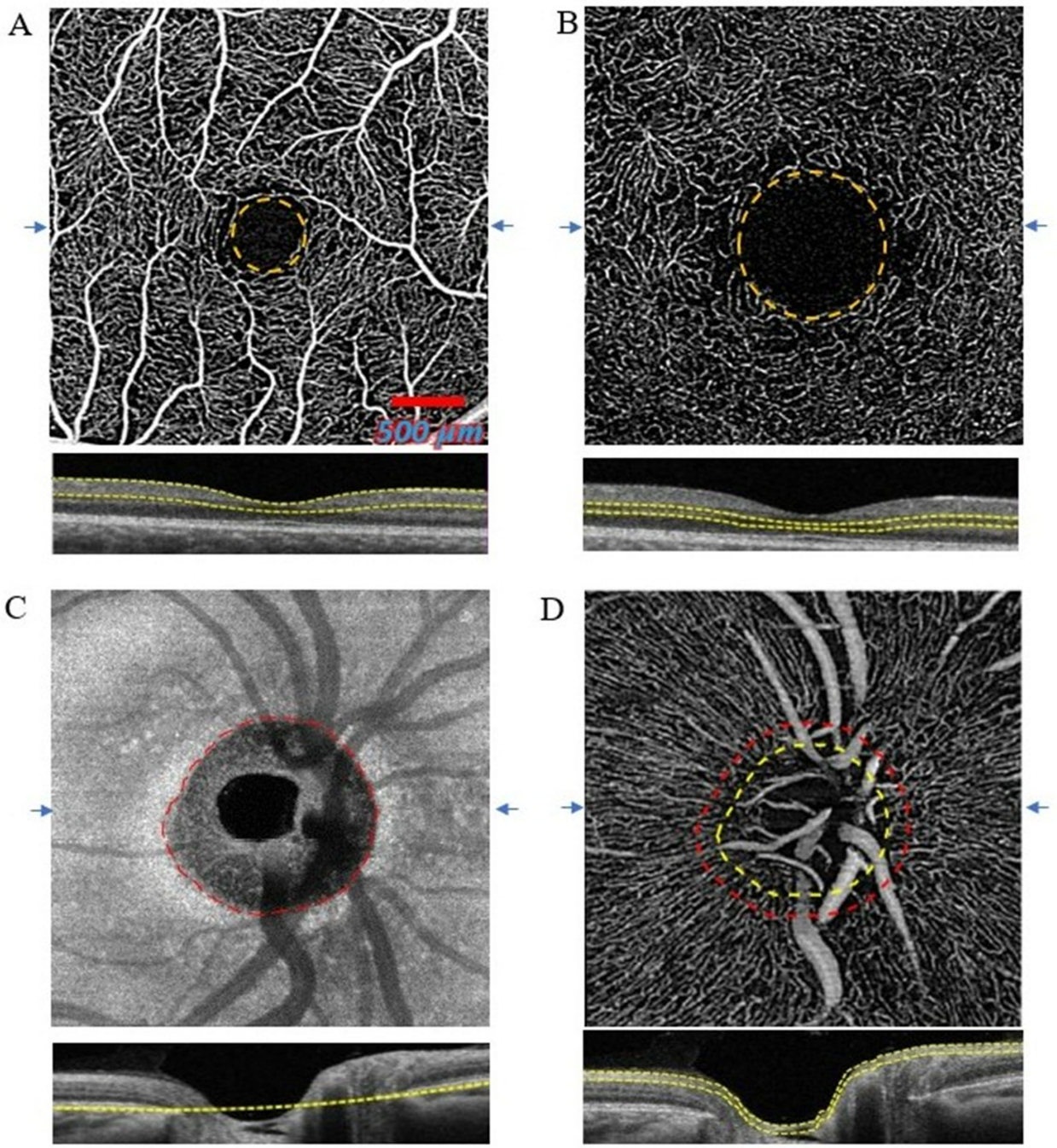

Figure 2. Excluding the influence of negative space (nonflow signal region) on the regional comparison of vascular reactivity. The central 0.5-mm and 1.00-mm diameter regions enclosed within the *yellow circles* on the macula superficial (**A**) and deep retinal layer (**B**) angiograms were excluded as negative space. The B-scans (along the *blue arrow markers*) are illustrated below the images and demonstrate the retinal slab segmented for generating the angiogram images. (**C**) An example of the retinal pigment epithelium (RPE) enface slab used for delineating the Bruch's membrane opening to guide the exclusion of negative space on the disc angiogram images. (**D**) An overlay of Bruch's membrane opening (in *red*) and the negative space region excluded from the disc analysis (in *yellow*). To ensure the inclusion of the radial vessels around the disc edge, the negative space excluded begins ~150 μm from the edge of the Bruch's membrane opening. The radial vessels were extracted from the superficial 75 μm of the OCTA at the disc.

A repeated-measures ANOVA was used for the comparison between layers.

Statistical analyses were performed using SPSS (IBM SPSS Statistics for Windows, version 27.0; IBM Corp, Armonk, NY, USA). Assumptions of normality were assessed using the Kolmogorov–Smirnov test. Mauchly's assessment of sphericity was used to assess the assumption of sphericity for interpreting the significance of the repeated-measures ANOVA. When the assumption of sphericity was violated, the *P* value associated with the Greenhouse–Geisser adjusted degree of freedom was reported. Statistical significance was defined at an α level of 0.05, and Bonferroni adjustments were

Investigative Ophthalmology & Visual Science

applied for multiple comparison. For example, in comparing the regional effect of the O_2 gas in the superficial retinal vasculature, which included a comparison of macula, temporal macula, and radial vessels, statistical significance was defined at an α level of 0.017.

Results

The participants examined in the study had no medical history of vascular disease. Of the eight participants studied, three self-reported as Asian, three as white or Caucasian, one as Hispanic or Latino, and one as African American or black. One participant had a history of caffeine intake on the day of the study. There were no adverse events or complaints during the administration of the protocol in this cohort, and no participant withdrew from the study.

The range of signal strength of the images analyzed was between 8 and 10, with the modal signal strength being 9 (Table). There was no trend toward weakening signal strength of the OCTA images between gas conditions such as during the O_2 breathing, which was last in the order of gas conditions induced (Table).

Characteristics and Reactivity of Intraretinal Vessels

The retinal capillary density at baseline (room air condition) differed by region and depth (Fig. 3). In the macula and temporal macula, higher VSD was observed in the superficial retinal layer compared to the deep retinal layer ($F(1, 7) = 157.83$, $P < 0.001$ for the superficial versus deep retinal layers of the macula; $F(1, 7) = 10.04$, $P = 0.016$ for the superficial versus deep retinal layers of the temporal macula). Among the superficial retinal layer only, the vessel density was highest in the macula region followed by the radial peripapillary vessels and then the temporal macula ($F(2, 7) = 15.55$, $P = 0.006$). Each pairwise comparison was

Table. Demographics of the Participants Studied and the Signal Strengths of the Images Analyzed Under the Various Gas Nonrebreathing Conditions

Demographics	Value
Number of participants	8
Age, mean (minimum, maximum), y	35 (24, 52)
Gender, female/male, *n*	3/5
Eyes, OS/OD, *n*	5/3
Blood pressure, mean (minimum, maximum), mm Hg	
Systolic	120 (112, 135)
Diastolic	80 (61, 85)
OCTA signal strength under gas nonrebreathing conditions, mean (minimum/maximum)	
Macula	
RA	9 (9, 10)
O_2	9 (9, 10)
O_2	9 (9, 10)
Temporal macula	
RA	9 (8, 10)
CO_2	9 (9, 10)
O_2	9 (9, 10)
Disc	
RA	9 (8, 9)
CO_2	9 (9, 10)
O_2	9 (8, 10)

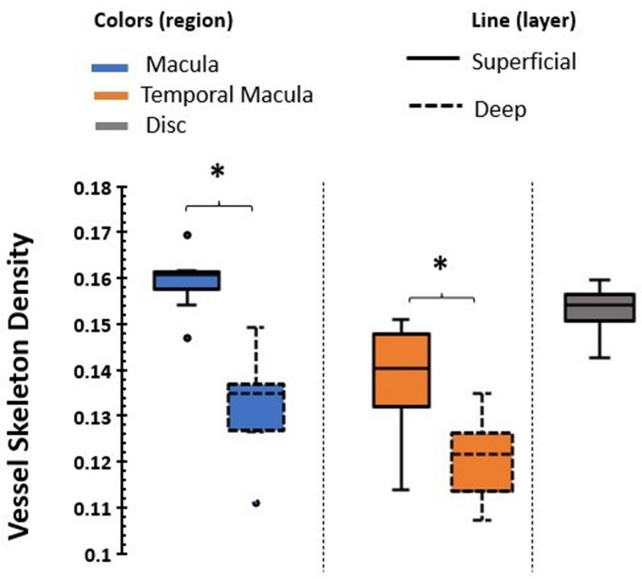

Figure 3. VSD of retinal vasculature by region and depth at baseline (room air). The retinal vessel density differed by region and depth, with the highest VSD measures in the superficial layers. Among the superficial layers (including the radial vessels), the VSD measures were the highest in the macula and radial peripapillary region compared to that of the temporal macula.

significantly different (macula versus temporal macula VSD, $P = 0.001$; macula versus radial peripapillary VSD, $P = 0.006$; radial peripapillary versus temporal macula VSD, $P = 0.001$). A similar tendency was observed in the deep retinal layer between the macula and the temporal macula VSD ($F(1, 7) = 5.01$, $P = 0.06$). When the analysis was repeated excluding the outliers (Fig. 3), the trends of the result were unchanged.

For all the retinal regions and layers assessed, the apparent VSD was qualitatively the highest during the CO_2 nonrebreathing condition and the lowest during the O_2 conditions (Fig. 4). Quantitatively, the VSD measures across conditions attributable to the gas breathing were significantly different ($F(2, 7) = 28.22$, $P < 0.001$ and $F(2, 7) = 33.81$, $P < 0.001$ for the gas effect on the superficial and deep retinal layer VSD, respectively; $F(2, 7) = 25.46$, $P < 0.001$ and $F(2, 7) = 51.20$, $P < 0.001$ for the superficial and deep temporal macula VSD, respectively; and $F(2, 7) = 30.69$, $P < 0.001$ for the radial peripapillary VSD; Fig. 5A). In terms of the proportion of change from baseline in the superficial retinal layer, the temporal macula showed a significantly greater total change than the macula and radial peripapillary vessels (15% change in temporal macula VSD compared to 8% and 7% change in the macula and radial peripapillary VSD) (Fig. 5B). The differences in the cumulative gas effect of the regional comparisons were mostly driven by the response to O_2 (10% change in temporal macula compared to 4% and 3% change in the macula and radial peripapillary vessels, respectively) (Fig. 5B).

A similar trend was present in the deep retinal layer of the macula and temporal macula comparison. There was a higher magnitude of cumulative gas effect in the temporal macula than the central macula (37% and 19% in the temporal macula and macula, respectively), and this change was primarily driven by the response to the O_2 (26% and 12% in the temporal macula and macula, respectively) (Fig. 5B). The analyses were repeated excluding the participant with

Investigative Ophthalmology & Visual Science

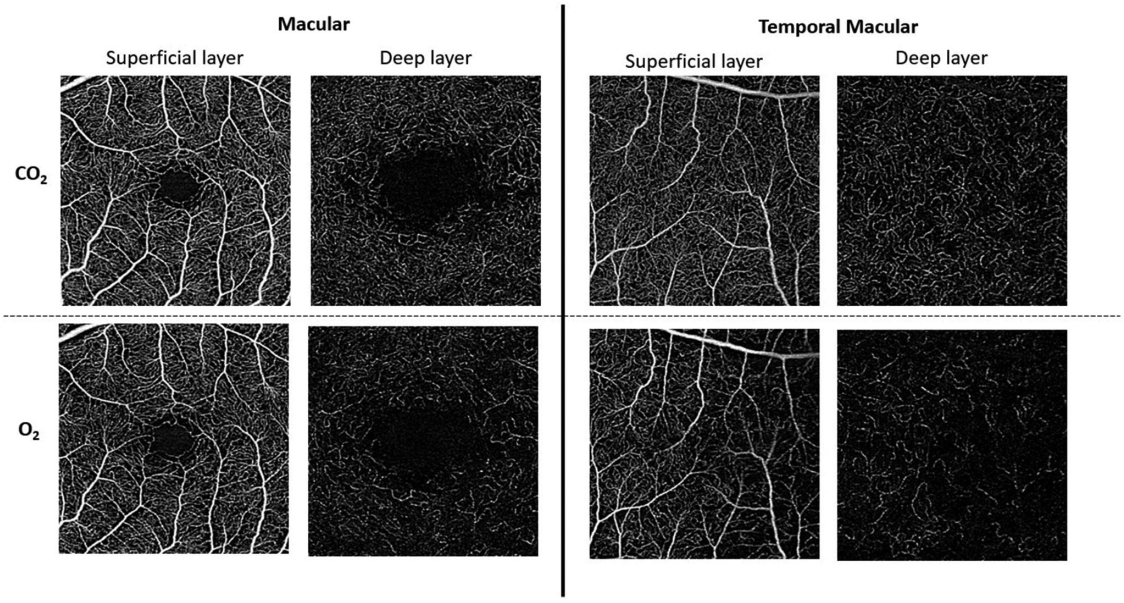

Figure 4. Regional and retinal layer vascular reactivity to O_2 and CO_2 conditions. The figure shows OCTA images of the macular and temporal macula during CO_2 and O_2 conditions from one participant. Vessel densities were greater during CO_2 conditions compared to O_2 conditions. For each region, the changes were greater in the deep layers compared to the superficial layers. Projection artifacts in the deep layers were extracted using the OCTA manufacturer's software. All images have signal strength of 10.

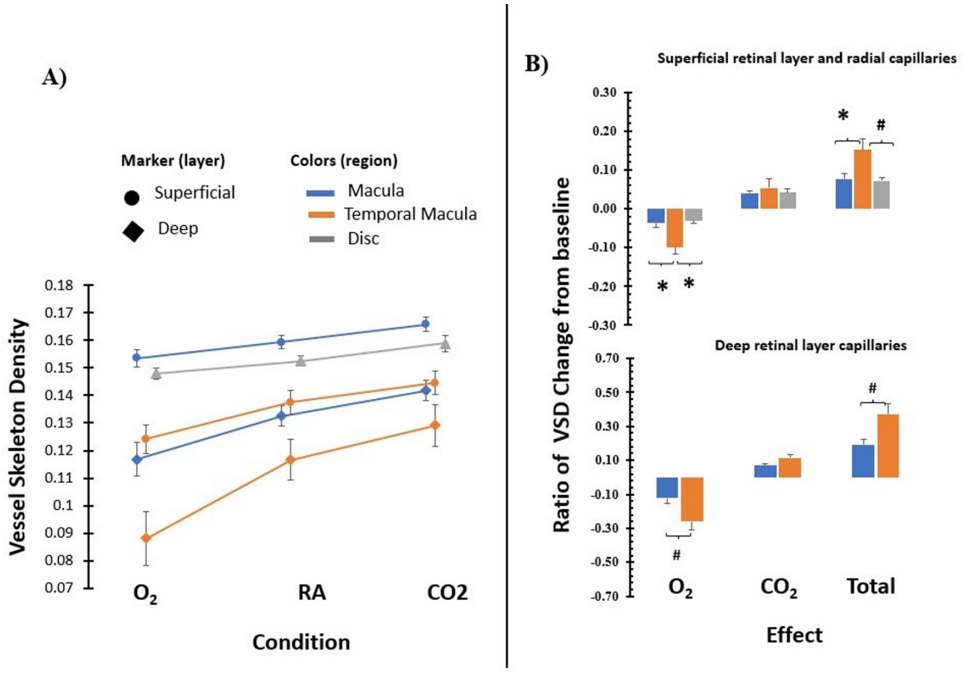

Figure 5. Regional analysis of retinal vascular reactivity. (**A**) Vessel skeleton density assessed at baseline (RA) as well as under 100% O_2 and 5% CO_2 gas conditions. (**B**) Ratio of change attributable to gas effects from baseline. The *error bars* are standard errors. *Define P values less than Bonferroni-adjusted P value (0.017). #Denotes an α level of $0.017 < P < 0.05$.

caffeine intake and adjusting for the effect of age as a covariant, and the trends of the result were similar.

Characteristics and Reactivity of Choriocapillaris

Unlike the retinal capillaries, there was no regional differences between FDD of the macula and temporal macula at baseline ($F(1, 7) = 0.40$, $P = 0.55$). There was also no difference in the MFDS ($F(1, 7) = 0.00$, $P = 1.00$) (Fig. 6). There was also no significant gas effect on FDD metric in the macula or the temporal macula regions ($F(2, 14) = 3.61$, $P = 0.054$ and $F(2, 14) = 1.92$, $P = 0.83$, respectively). However, there was a significant gas effect for the MFDS in the macula ($F(2, 14) = 4.57$, $P = 0.032$) and temporal macula

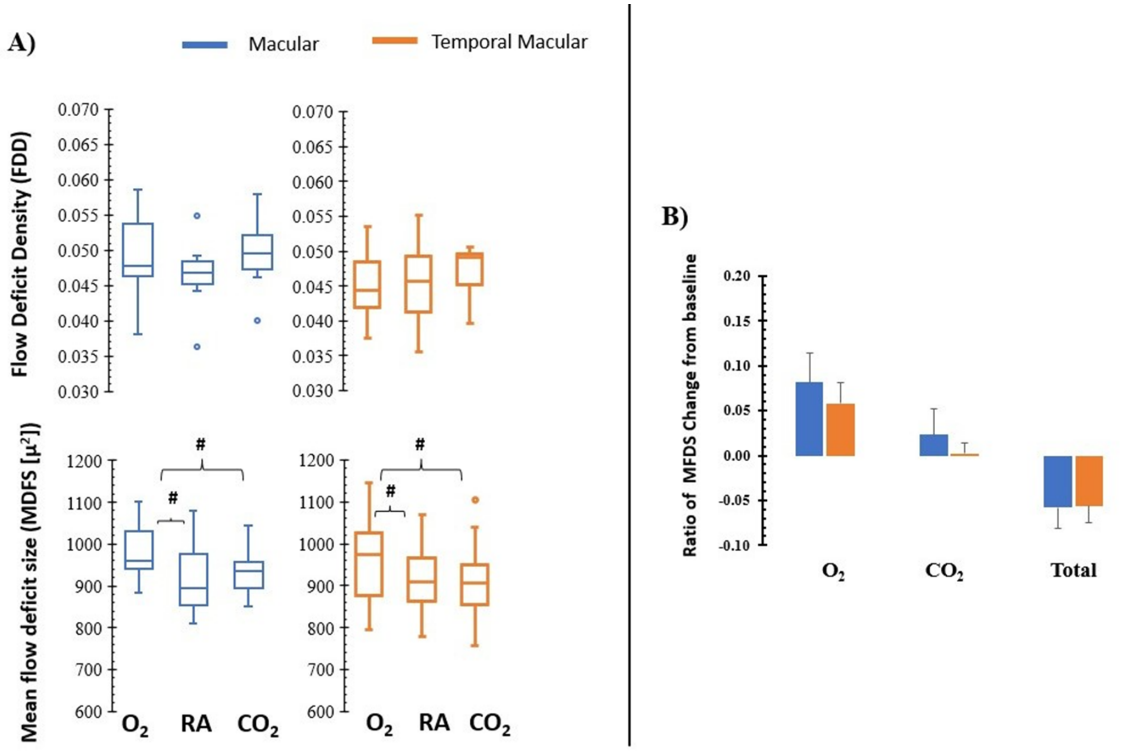

Figure 6. Choriocapillaris response to gas perturbation. (**A**) Box-and-whisker plots of the FDD and MFDS of the choriocapillaris. The FDD did not show gas-induced changes while the MFDS metric trended toward significance in response to O_2. (**B**) The proportion of the MFDS change from baseline was similar between the macula and temporal macula regions. The *error bars* are standard errors. #Denotes an α less than 0.05 but greater than the Bonferroni-adjusted *P* value (0.017).

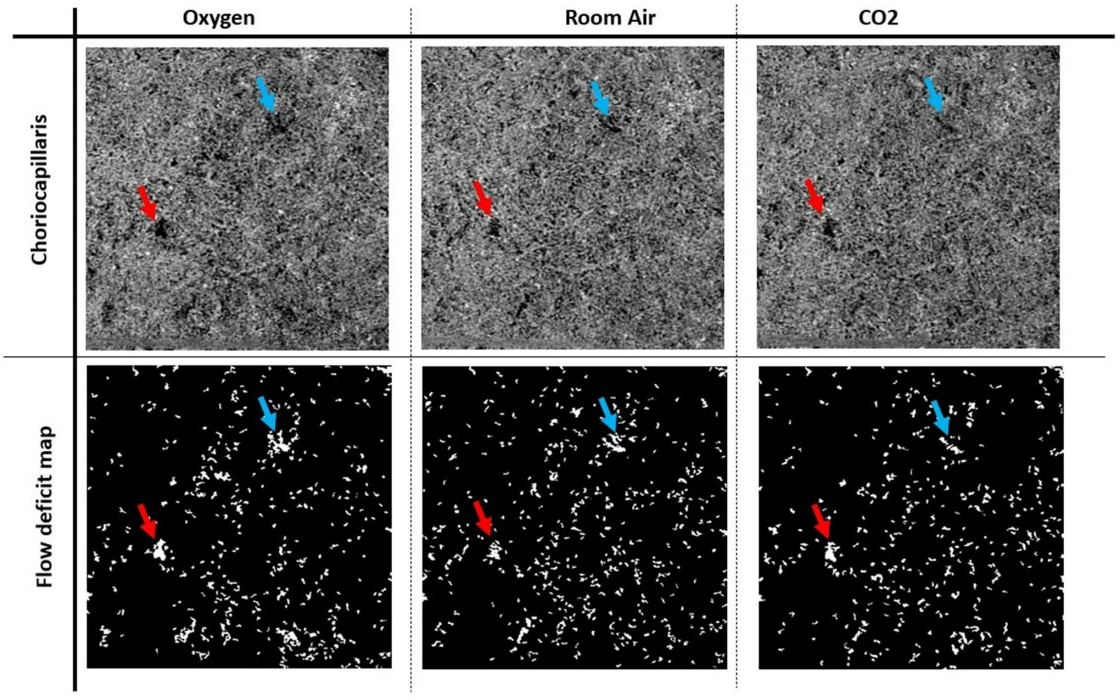

Figure 7. Choriocapillaris reactivity to gas perturbation. The flow deficit size of the choriocapillaris (shown with the *arrows*) was larger during the O_2 nonrebreathing as compared to during room air and CO_2 nonrebreathing.

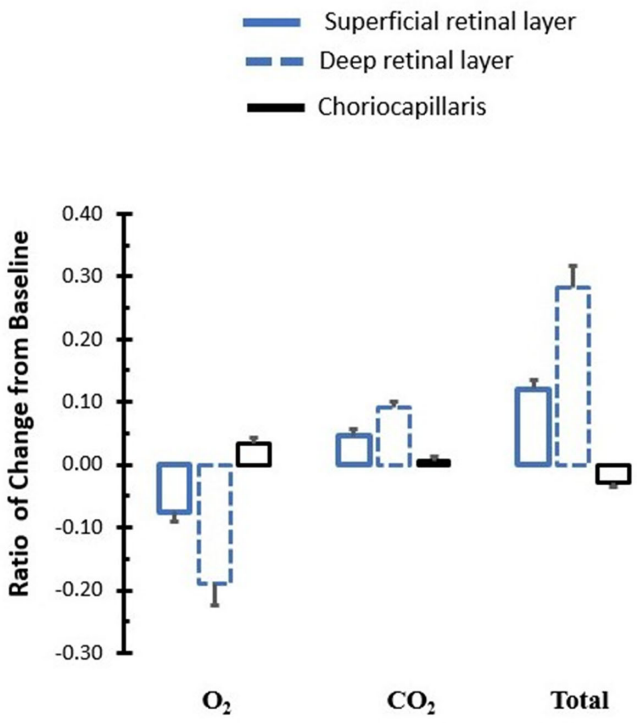

Figure 8. Layer-specific reactivity. The figure shows the retinal capillaries and choriocapillaris response to the gas conditions. The deep retinal layer VSD showed the largest changes from baseline followed by the superficial retinal layer VSD, in which O_2 caused a decrease in vessel density. The choriocapillaris had the least magnitude of gas response from baseline in which O_2 caused a decrease in mean flow deficit size from baseline. The cumulative gas responses were computed as the difference between the CO_2 and O_2 measures divided by the room air measure. The *error bars* are standard errors.

($F(2, 14) = 6.02$, $P = 0.013$) (Fig. 6). Qualitatively larger FDs were seen in the choriocapillaris images during O_2 than during CO_2 breathing (Fig. 7). The total gas effect was similar between the macula (5.8%) and temporal macula (5.6%) ($F(1, 7) = 0.01$, $P = 0.93$).

Layer-Specific Reactivity of the Retinal Vascular and Choriocapillaris

The magnitude of total vascular response to the gas conditions varied between the retinal capillaries and the choriocapillaris (Fig. 8). The deep retinal layer showed the greatest total gas effect, with up to 66% contributed by the response to O_2. This was followed by the response in the superficial retinal layer, which also showed a significantly greater total gas effect than the choriocapillaris. Similar to the deep retinal layer, close to 66% of the total response of the superficial layer was also contributed by the response to O_2. The choriocapillaris showed the least magnitude of response to the gas conditions, with the MFDS increasing during the O_2 condition and no response to the CO_2 conditions.

Discussion

We investigated the characteristics of the superficial and deep retinal layer capillaries as well as the choriocapillaris in the macula, temporal macula, and radial peripapillary region. Our results demonstrate heterogeneous capillary density and function of the retina by region and layer. The FDD and MFDS of the choriocapillaris were less heterogeneous. When physiologic changes in blood oxygen and carbon dioxide levels were induced by gas breathing, the largest vascular response was found in the deep retinal layer, followed by the superficial retinal layer. The choriocapillaris was the least responsive to the gas conditions. These studies demonstrate the reactivity of the retinal capillaries and choriocapillaris in the same group of participants in vivo and across different regions of the retina and are distinct from previous studies of large-caliber vessels and regional oxygen distribution.[2,11,28] Unlike Trick et al.,[11] we found significant spatial heterogeneity to hyperoxia in both the superficial and deep retinal layers of healthy volunteers, with vessels in the temporal macula region showing the largest responses. This may be potentially explained by the differences in imaging resolution between the devices used for the retinal assessments.

The differences we observe between the choriocapillaris and retinal capillary response to O_2 and CO_2 breathing confirm some of the known physiology of these vascular networks and also provide new insights that may be relevant for understanding disease pathophysiology. For example, the sheathing of the retinal capillaries with pericytes presumably provides contractile and dilatory ability that is not possible in the choriocapillaris.[35–37] The known difference in pericyte distribution and function across vascular segments may serve as the physiologic basis for the observed differences in the retinal capillary responses.[7,8] In addition, flow in the choriocapillaris is thought to be mainly regulated through autonomic innervation while that of the retinal vessels is adapted for detecting and adjusting to local factors including O_2 or CO_2.[38] On the other hand, it is not immediately clear why the deep retinal layer demonstrates larger magnitude of VSD change in response to O_2 or CO_2. However, our findings are consistent with at least one other study that demonstrated increased vascular responsiveness to hyperoxia in the deep retinal capillaries.[39] One possibility is that the proximity of the deep retinal layer capillaries to the choriocapillaris may result in more dramatic changes in oxygen tension in the outer retina and correspondingly larger changes in perfusion of those capillaries.

We demonstrate that it is feasible to perform layer-specific analysis of the retinal and choriocapillaris vasculature[18,40] and also assess the reactivity of the vascular network in a regional manner using commercially available SS-OCTA. Retinal vascular reactivity assessment has the potential to elucidate vascular abnormalities before the classic signs of vascular abnormalities such as capillary nonperfusion, microaneurysms, or hemorrhage. In diabetes, it may capture endothelial or pericyte cell dysfunction, and in hypertension, it may capture sclerosing of the vascular wall.[18,23,41,42] Furthermore, the ability to compare the regional and retinal sublayer properties of vascular reactivity assessment may help refine the methods for investigating the retinal manifestation of disease with spatial bias such as in glaucoma, diabetes, sickle cell disease, and other systemic or neurologic disease.[43,44]

Our study is potentially confounded by factors including smoking status and use of vasoconstrictors like phenylephrine for pupillary dilation. Other limitations include the number of participants and the method of vascular stimulation. However, the effect sizes we observed are very large and significant. Our findings are also consistent and

Investigative Ophthalmology & Visual Science

explained by trends reported by the previous studies.[18,23,39] Although we did not assess end-tidal CO_2 during the gas inhalation, the method used in the study has been very well characterized by Yezhuvath et al.,[25] from whom we adopted the procedure. For example, Yezhuvath et al.[25] found that after 60 seconds of CO_2 nonbreathing, the end-tidal CO_2 significantly increased by 28% while the arterial oxygen saturation only decreased by 0.1%. Heart rate and breathing rate were unchanged.[25,45] In addition, Yezhuvath and colleagues[25] reported that 1 minute of 5% CO_2 gas breathing (which is much more comfortable for human participants) yielded similar cerebrovascular reactivity as 4 minutes. Given the essentially identical approach we use, we do not expect the physiologic changes induced by the gas breathing in our study to significantly differ from that already reported in the literature.[25,45] Furthermore, this gas inhalation method has been validated across hundreds of participants and is being used in a multicenter study as a lead candidate for a biomarker of cerebrovascular reactivity.[18,23,26,27] While this gas provocation approach has proven effective, it may benefit from additional systemic evaluations such as $PaCO_2$, PaO_2, and pH. In the unlikely case that any of our healthy human volunteers (with no known respiratory conditions) were underventilating for some reason, our results would be an underestimate of the true effect of the gas stimuli. Additional studies comparing the blood flow response measured with OCTA and systemic blood oxygen levels in both healthy participants and those with vascular disease will be helpful. Other methods of vascular stimulation, including light–dark adaptation and flickering light, can also complement our understanding of the retinal vascular physiology in future studies.[20,46–48]

In conclusion, we report that retinal vascular function demonstrates significant regional and layer-specific heterogeneity while choriocapillaris function has much less heterogeneity. To date, there are no other in vivo human studies that provide simultaneous assessment of retinal vascular and choricapillaris reactivity at the capillary level as is done in this study. Ex vivo experiments and animal models have demonstrated the potential heterogeneous nature of a vascular response to global stimulations, and our work clearly demonstrates this differential responsiveness of the retinal and choriocapillaris vasculature in vivo for the first time. Future studies assessing the nature of these responses to other stimuli, including flickering light or autonomic innervations, as well as a combination of stimuli, may help further elucidate the mechanisms of retinal disease processes.

Acknowledgments

Supported by a National Institutes of Health grant to AHK (R01EY030564) as well as unrestricted departmental support from Research to Prevent Blindness.

Disclosure: **B.S. Ashimatey**, None; **X. Zhou**, None; **Z. Chu**, None; **M. Alluwimi**, None; **R.K. Wang**, Carl Zeiss Meditec (F); **A.H. Kashani**, Carl Zeiss Meditec (F)

References

1. Remington LA. *Retina, Clinical Anatomy and Physiology of the Visual System* (Third ed). St. Louis, MO: Butterworth-Heinemann; 2012:87–88.
2. Kur J, Newman EA, Chan-Ling T. Cellular and physiological mechanisms underlying blood flow regulation in the retina and choroid in health and disease. *Prog Retin Eye Res*. 2012;31(5):377–406.
3. Hayreh SS. Physiological anatomy of the retinal vasculature. In: Dartt DA , ed. *Encyclopedia of the Eye*. Oxford, UK: Academic Press; 2010:431–438.
4. Matsunaga D, Yi J, Puliafito CA, Kashani AH. OCT angiography in healthy human subjects. *Ophthalmic Surg Lasers Imaging Retina*. 2014;45(6):510–515.
5. Campbell JP, Zhang M, Hwang TS, et al. Detailed vascular anatomy of the human retina by projection-resolved optical coherence tomography angiography. *Sci Rep*. 2017;7:42201.
6. Lavia C, Mecê P, Nassisi M, et al. Retinal capillary plexus pattern and density from fovea to periphery measured in healthy eyes with swept-source optical coherence tomography angiography. *Sci Rep*. 2020;10(1):1474.
7. Yu PK, Yu D, Alder VA, Seydel U, Su E, Cringle SJ. Heterogeneous endothelial cell structure along the porcine retinal microvasculature. *Exp Eye Res*. 1997;65(3):379–389.
8. Matsushita K, Puro DG. Topographical heterogeneity of K(IR) currents in pericyte-containing microvessels of the rat retina: Effect of diabetes. *J Physiol*. 2006;573(pt 2):483–495.
9. Hormel TT, Jia Y, Jian Y, et al. Plexus-specific retinal vascular anatomy and pathologies as seen by projection-resolved optical coherence tomographic angiography. *Prog Retin Eye Res*. 2020;80:100878.
10. Lavia C, Couturier A, Erginay A, Dupas B, Tadayoni R, Gaudric A. Reduced vessel density in the superficial and deep plexuses in diabetic retinopathy is associated with structural changes in corresponding retinal layers. *PLoS One*. 2019;14(7):e0219164.
11. Trick GL, Edwards P, Desai U, Berkowitz BA. Early supernormal retinal oxygenation response in patients with diabetes. *Invest Ophthalmol Vis Sci*. 2006;47(4):1612–1619.
12. Kern TS, Engerman RL. Vascular lesions in diabetes are distributed non-uniformly within the retina. *Exp Eye Res*. 1995;60(5):545–549.
13. Tang J, Mohr S, Du YD, Kern TS. Non-uniform distribution of lesions and biochemical abnormalities within the retina of diabetic humans. *Curr Eye Res*. 2003;27(1):7–13.
14. Linz MO, Scott AW. Wide-field imaging of sickle retinopathy. *Int J Retina Vitreous*. 2019;5(suppl 1):27.
15. Dimitrova G, Chihara E. Implication of deep-vascular-layer alteration detected by optical coherence tomography angiography for the pathogenesis of diabetic retinopathy. *Ophthalmologica*. 2019;241(4):179–182.
16. Simonett JM, Scarinci F, Picconi F, et al. Early microvascular retinal changes in optical coherence tomography angiography in patients with type 1 diabetes mellitus. *Acta Ophthalmol*. 2017;95(8):e751–e755.
17. Meshi A, Chen KC, You QS, et al. Anatomical and functional testing in diabetic patients without retinopathy: Results of optical coherence tomography angiography and visual acuity under varying contrast and luminance conditions. *Retina*. 2019;39(10):2022–2031.
18. Singer M, Ashimatey BS, Zhou X, Chu Z, Wang R, Kashani AH. Impaired layer specific retinal vascular reactivity among diabetic subjects. *PLoS One*. 2020;15(9):e0233871.
19. Ashraf M, Sampani K, Clermont A, et al. Vascular density of deep, intermediate and superficial vascular plexuses are differentially affected by diabetic retinopathy severity. *Invest Ophthalmol Vis Sci*. 2020;61(10):53.
20. Penas S, Araújo T, Mendonça AM, et al. Retinal and choroidal vasoreactivity in central serous chorioretinopathy. *Graefes Arch Clin Exp Ophthalmol*. 2022;260(12):3825–3836.
21. Flammer J, Orgül S, Costa VP, et al. The impact of ocular blood flow in glaucoma. *Prog Retin Eye Res*. 2002;21(4):359–393.

Investigative Ophthalmology & Visual Science

22. Hood DC, Raza AS, de Moraes CG, Liebmann JM, Ritch R. Glaucomatous damage of the macula. *Prog Retin Eye Res*. 2013;32:1–21.
23. Ashimatey BS, Green KM, Chu Z, Wang RK, Kashani AH. Impaired retinal vascular reactivity in diabetic retinopathy as assessed by optical coherence tomography angiography. *Invest Ophthalmol Vis Sci*. 2019;60(7):2468–2473.
24. Kushner-Lenhoff S, Ashimatey BS, Kashani AH. Retinal vascular reactivity as assessed by optical coherence tomography angiography. *J Vis Exp*. 2020;157:10.3791/60948.
25. Yezhuvath US, Lewis-Amezcua K, Varghese R, Xiao G, Lu H. On the assessment of cerebrovascular reactivity using hypercapnia BOLD MRI. *NMR Biomed*. 2009;22(7):779–786.
26. Liu P, De Vis JB, Lu H. Cerebrovascular reactivity (CVR) MRI with CO2 challenge: A technical review. *Neuroimage*. 2019;187:104–115.
27. Lu H, Kashani AH, Arfanakis K, et al. MarkVCID cerebral small vessel consortium: II. Neuroimaging protocols. *Alzheimers Dement*. 2021;17(4):716–725.
28. Tayyari F, Venkataraman ST, Gilmore ED, Wong T, Fisher J, Hudson C. The relationship between retinal vascular reactivity and arteriolar diameter in response to metabolic provocation. *Invest Ophthalmol Vis Sci*. 2009;50(10):4814–4821.
29. Mo S, Phillips E, Krawitz BD, et al. Visualization of radial peripapillary capillaries using optical coherence tomography angiography: The effect of image averaging. *PLoS One*. 2017;12(1):e0169385.
30. Kim AY, Rodger DC, Shahidzadeh A, et al. Quantifying retinal microvascular changes in uveitis using spectral-domain optical coherence tomography angiography. *Am J Ophthalmol*. 2016;171:101–112.
31. Chu Z, Lin J, Gao C, et al. Quantitative assessment of the retinal microvasculature using optical coherence tomography angiography. *J Biomed Opt*. 2016;21(6):66008.
32. Chu Z, Zhang Q, Gregori G, Rosenfeld PJ, Wang RK. Guidelines for imaging the choriocapillaris using OCT angiography. *Am J Ophthalmol*. 2020;222:92–101.
33. Zhang Q, Zheng F, Motulsky EH, et al. A novel strategy for quantifying choriocapillaris flow voids using swept-source OCT angiography. *Invest Ophthalmol Vis Sci*. 2018;59(1):203–211.
34. Chu Z, Zhou H, Cheng Y, Zhang Q, Wang RK. Improving visualization and quantitative assessment of choriocapillaris with swept source OCTA through registration and averaging applicable to clinical systems. *Sci Rep*. 2018;8(1):16826.
35. Frank RN, Turczyn TJ, Das A. Pericyte coverage of retinal and cerebral capillaries. *Invest Ophthalmol Vis Sci*. 1990;31(6):999–1007.
36. Cavallotti C, Corrado BG, Feher J. The human choriocapillaris: Evidence for an intrinsic regulation of the endothelium? *J Anat*. 2005;206(3):243–247.
37. Tilton RG, Miller EJ, Kilo C, Williamson JR. Pericyte form and distribution in rat retinal and uveal capillaries. *Invest Ophthalmol Vis Sci*. 1985;26(1):68–73.
38. Delaey C, Van De Voorde J. Regulatory mechanisms in the retinal and choroidal circulation. *Ophthalmic Res*. 2000;32(6):249–256.
39. Hagag AM, Pechauer AD, Liu L, et al. OCT angiography changes in the 3 parafoveal retinal plexuses in response to hyperoxia. *Ophthalmol Retina*. 2018;2(4):329–336.
40. Hommer N, Kallab M, Sim YC, et al. Effect of hyperoxia and hypoxia on retinal vascular parameters assessed with optical coherence tomography angiography. *Acta Ophthalmol*. 2022;100(6):e1272–e1279.
41. Cogan DG, Toussaint D, Kuwabara T. Retinal vascular patterns. IV. Diabetic retinopathy. *Arch Ophthalmol*. 1961;66:366–378.
42. Sieker HO, Hickam JB. Normal and impaired retinal vascular reactivity. *Circulation*. 1953;7(1):79–83.
43. Blanks JC, Schmidt SY, Torigoe Y, Porrello KV, Hinton DR, Blanks RH. Retinal pathology in Alzheimer's disease. II. Regional neuron loss and glial changes in GCL. *Neurobiol Aging*. 1996;17(3):385–395.
44. Chung HS, Harris A, Halter PJ, et al. Regional differences in retinal vascular reactivity. *Invest Ophthalmol Vis Sci*. 1999;40(10):2448–2453.
45. Lu H, Liu P, Yezhuvath U, Cheng Y, Marshall O, Ge Y. MRI mapping of cerebrovascular reactivity via gas inhalation challenges. *J Vis Exp*. 2014(94):52306, doi:10.3791/52306.
46. Longo A, Geiser M, Riva CE. Subfoveal choroidal blood flow in response to light-dark exposure. *Invest Ophthalmol Vis Sci*. 2000;41(9):2678–2683.
47. Warner RL, de Castro A, Sawides L, et al. Full-field flicker evoked changes in parafoveal retinal blood flow. *Sci Rep*. 2020;10(1):16051.
48. Fitzgerald ME, Gamlin PD, Zagvazdin Y, Reiner A. Central neural circuits for the light-mediated reflexive control of choroidal blood flow in the pigeon eye: A laser doppler study. *Vis Neurosci*. 1996;13(4):655–669.

Investigative Ophthalmology & Visual Science